Micromagnetic Modelling of Hysteresis in Permalloy Thin Films with Non-Magnetic Defects

Inna Lobanova, Stéphane Labbé, Stéphane Despréaux

APPLICATIONS OF
MODELLING AND SIMULATION
http://arqiipubl.com/ams eISSN 2600-8084 VOL 6, 2022, 115-121

Micromagnetic Modelling of Hysteresis in Permalloy Thin Films with Non-Magnetic Defects

I. I. Lobanova[1,3*], S. Labbé[2] and S. Despréaux[3]

[1]Université Grenoble Alpes, Grenoble, France
[2]Sorbonne Université, CNRS, Université de Paris, Laboratoire Jacques-Louis Lions (LJLL), Paris, France
[3]Laboratoire Jean Kuntzmann, CNRS, Grenoble, France

[*]Corresponding author: inna.lobanova@univ-grenoble-alpes.fr

Submitted 06 July 2022, Revised 28 August 2022, Accepted 03 September 2022, Available online 08 September 2022.

Abstract: In this paper, we present the results of numerical micromagnetic modelling of the domain wall pinning on non-magnetic defects in a ferromagnetic thin sheet of permalloy. We compared the influence of different distribution of non-magnetic inclusions on the magnetization reversal in case of uniaxial anisotropy. It is shown that the non-magnetic defects help to resolve vortex singularities and play a role of pinning states. It is demonstrated that the defects located on the sides of the sheet favor the transition into the single-domain state. By varying the in-plane anisotropy constant, we observed that the defects located in the center lead to higher coercivity, $\boldsymbol{H_c}$ when the domain wall width is comparable to the size of the sample, but narrowing of domain wall width leads to a change of energetically favorable distribution of defects and the highest $\boldsymbol{H_c}$ is when defects are located on the sides. It is shown that the defects located in the corner of the sheet serve as nucleation points for the magnetization reversal process and have a lower threshold for unpinning of the domain walls.

Keywords: Domain walls movement; Hysteresis; Micromagnetic modelling; Soft magnetic materials; Spintronics.

1. INTRODUCTION

The hysteresis process and magnetization reversal in ferromagnetic permalloy thin films are widely studied due to their value to fundamental research and their potential application in future high density non-volatile data storage devices [1-7]. Those processes are influenced by the presence of defects, which are unavoidable in real materials. Therefore, it is of great interest to study the influence of the defects on the magnetic structure. In this article, we focus on the idealized, thermal hysteresis, which is in itself interesting as a prerequisite to building a model that takes into account thermal effects.

The phenomenon of hysteresis is intimately linked with the microscopic processes occurring in a magnetic body and concerns the manner in which the magnetization is reversed due to the application of an external magnetic field [8]. This relates not only to the direction in which the field is applied, but also to the specific magnetic state of the sample, which depends on the magnetic history and the particular configuration/distribution of the magnetic spins. Also, of importance will be the purity and crystallinity of the sample itself. In particular, impure samples and grain boundaries will have a significant influence on the manner in which ferromagnetic domain walls are nucleated and how they propagate [9,10].

A magnetic domain wall is a region of transition in which the atomic magnetic moments vary smoothly in orientation from one magnetic domain to a neighboring domain. The width of the domain wall corresponds to the energy associated with neighboring magnetic moments. When the moments are non-collinear, they have higher exchange energy, and when they are not aligned with the easy axis as defined by the magneto-crystalline energy, the latter has higher values. In addition to that, the macroscopic external and demagnetization fields influence the magnetization distribution in the body and also contribute to the domain wall formation and motion. The equilibrium state of a ferromagnet corresponds to the minimum of the full energy, that is a sum of these contributions [11, 12]. The detailed model will be explained in the next section.

Micromagnetic simulation is an efficient tool for studying various physical phenomena in thin magnetic films [13-17]. In this paper, using micromagnetic simulation, we analyze the influence of non-magnetic defects on the formation of domain structure and magnetization reversal in thin permalloy films with uniaxial in-plane magnetic anisotropy. The work consists of two parts: First, we analyzed the variation of the shape of the hysteresis cycle of a permalloy with increasing crystalline anisotropy, e.g. with decreasing domain wall width. Second, we compared materials with different exchange length to sample size ratio. In both cases the pattern of non-magnetic defects plays an important role as illustrated by the presented results.

2. MODELS AND SIMULATION DETAILS

Micromagnetics and domain theory are based on the same variational principle, which is derived from thermodynamic principles, as established initially in [18] and as reviewed in articles [11, 12]. According to this principle, the vector field of magnetization directions $\boldsymbol{m}(\boldsymbol{r}) = \boldsymbol{M}(\boldsymbol{r})/M_s$ is chosen so that the total free energy reaches an absolute or relative minimum under the constraint $|\boldsymbol{m}| = 1$, where $\boldsymbol{M}$ is magnetization vector and M_s is the value of magnetization at saturation.

We must distinguish between local and non-local magnetic energy terms. The local terms are based on energy densities, which are given by the local values of the magnetization direction only. The two non-local energy contributions are the stray field energy and the magnetostrictive self-energy. These energy terms give rise to torques of the magnetization vector that depend at any point on the magnetization directions at every other point. In the current article we consider the material as a permalloy and do not take into account the magnetostriction.

The fundamental property of a ferromagnet is its preference for a constant equilibrium magnetization direction. Deviations from this ideal case invoke an energy penalty, which can be described by the "stiffness" expression [18]:

$$E_{ex} = A\int |\nabla \boldsymbol{m}|^2 dV, \tag{1}$$

where A is a material constant, the so-called exchange stiffness constant, and V is the volume. The exchange energy (1) is isotropic because it is locally independent of the magnetization direction rotations. Even if the Heisenberg interaction between localized spins is not applicable (as in metallic ferromagnets), Equation (1) still describes phenomenologically the stiffness effect to first order.

The energy of a ferromagnet depends on the direction of the magnetization relative to the structural axes of the material. This dependence, which basically results from spin-orbit interactions, is described by the anisotropy energy. Considering the computation time, in the following article we focused on the uniaxial crystal anisotropy that is described by the following equation:

$$E_{ani} = K_u\int \sin^2\theta_M dV, \tag{2}$$

where K_u is uniaxial anisotropy constant, and θ_M is the angle between the easy axis and the particle's magnetization.

The magnetic field energy can be separated into two parts, the external field energy and the stray field energy. The first part, the interaction energy of the magnetization vector field with an external field $\boldsymbol{H}_{ext}$, is simply:

$$E_{Zeeman} = -\mu_0\int \boldsymbol{H_{ext}}\cdot \boldsymbol{M}\, dV. \tag{3}$$

where μ_0 is the vacuum permeability constant The second part of the magnetic field energy is the stray field $\boldsymbol{H}_\mathbf{d}$, a quasi-static electromagnetic contribution. The energy connected to it is:

$$E_d = -\tfrac{1}{2}\mu_0\int \boldsymbol{H_d}.\boldsymbol{M}\, dV. \tag{4}$$

The total magnetic energy E is the sum of the aforementioned contributions (Equations (1)-(4)). The basic problem consists in finding the minimum of this energy at each step of the external magnetic field of the magnetization cycle, which allows to derive the magnetic hysteretic behavior [11]. The computation of the equilibrium magnetization state is a relaxation process that is based on solving the Landau-Lifshitz (LL) partial differential equation that describes the evolution of $\boldsymbol{M}$ in time [18]. The described mathematical model has been implemented in a self-written software EMicroM by using specific numerical methods [19-22]. The schematic algorithm is given in Figure 1.

The first step is calculating the effective magnetic field $\boldsymbol{H}$, a key quantity of the micromagnetic theory, based on the initial magnetization field $\boldsymbol{M}(t=0)$ (input data). It is defined as the negative functional derivative of the free energy E with respect to $\boldsymbol{M}$, i.e.

$$\boldsymbol{H}(\boldsymbol{M}) = -\frac{1}{\mu_0}\frac{\delta E}{\delta \boldsymbol{M}} \tag{5}$$

It has the physical dimensions of a magnetic field (A/m) and can be understood as the local field affected by the magnetization. Then the variation of $\boldsymbol{M}$ is estimated according to LL equation and the corresponding energy is calculated. The magnetization $\boldsymbol{M}(t+dt)$ is computed by using the 2-order Taylor expansion. The energy can be approximated by 4-order polynomial and the optimal dt for the energy minimization can be calculated explicitly. The relaxation is reached when the variation of either the magnetization or the energy is below the threshold, ε or the maximum number of iterations is executed (input parameters).

The most challenging part of the modelling process is the computation of the demagnetizing field $\boldsymbol{H}_d$. The problem is discretized by using a Finite Volume Approximation which preserves the main properties of the operator given in the continuous model: positivity and symmetry [20, 22]. Furthermore, because of regular 3D grid, the resulting system has a block-Toeplitz structure, which allows to build fast solving method [23]. Based upon the use of fast Fourier transform, this method allows to reduce the computational cost from n^2 to $O(n\log(n))$ as well as to reduce the storage to $O(n)$ instead of n^2, where n is the number of cells in the grid [22, 23].

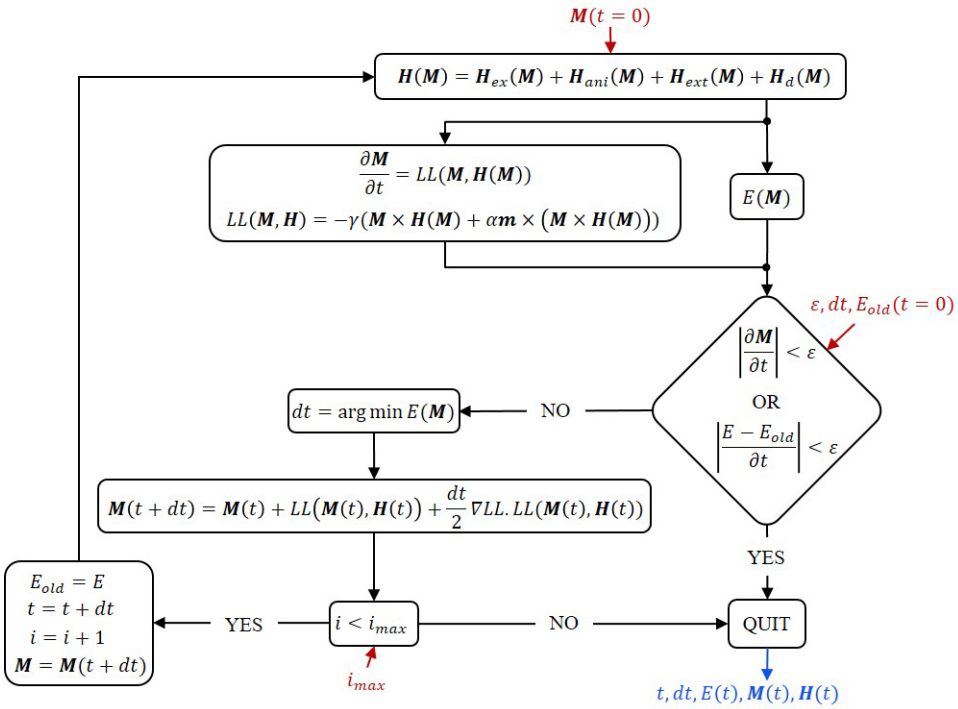

Figure 1. Schematic representation of the relaxation algorithm (see text for details). The input data are given in red and the output data are given in blue.

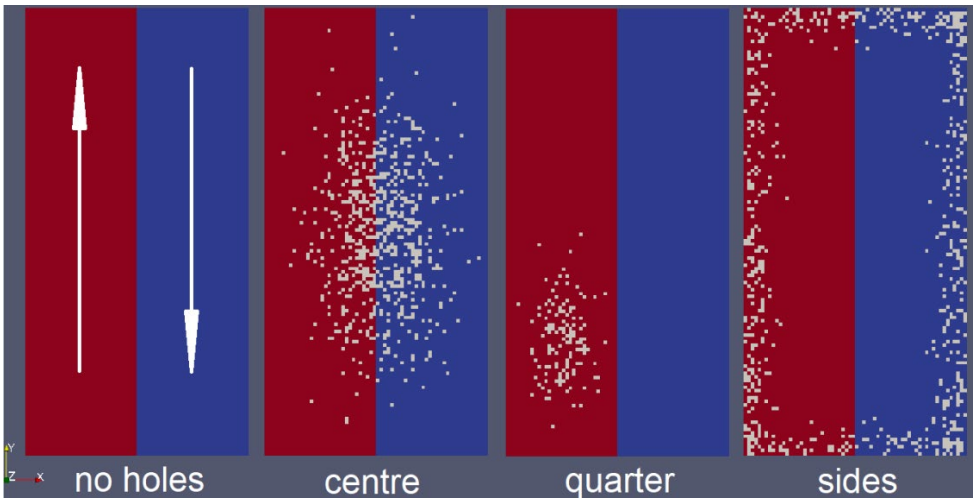

Figure 2. Sample geometry. From left to right: Initial geometry without defects, with defects in centre, quarter and sides. The initial magnetization is the same for all samples and presented by colour and arrows. The defects are presented as white dots.

We performed computations on ferromagnetic permalloy thin sheets with uniaxial in-plane anisotropy without taking into account magnetostriction effects. The representative volume element is a rectangular sheet with the following dimensions: width (X) 0.64 µm, length (Y) 1.28 µm and height (Z) 0.01 µm, meshed with 256×512×4 cubic cells. The easy axis is [010] direction and parallel to the applied magnetic field. The defects are represented by non-magnetic cells, simply referred as "holes" and their distribution is presented in Figure 2. The typical size of the non-magnetic defect is about $(10\ \text{nm})^3$. Material parameters used in the computation are presented in Table 1. In order to test numerically the influence of the defects on the stability of domain walls, we have run a relaxation process from an initial up-down magnetic state: Half of magnetization vectors are parallel to the *Y* axis (which coincides with the length of the sample) and another half is antiparallel (see Figure 2).

3. RESULTS AND DISCUSSION

3.1 Variation of Exchange Length to Sample Length Ratio

Varying only the exchange length allows to "scale" the exchange length to sample length ratio. In our computation we used the exchange stiffness constant *A* as a tuning parameter. We would like to note that in real materials those values may be much lower, in this case it is necessary to simply adapt the size of the sample to obtain the same exchange length to sample length ratio.

Table 1. Material parameters

	S1	S2	S3	
M_s	800	800	800	Magnetization, kA/m
K_u	0.5	0.5	100	Anisotropy constant, kJ/m^3
A	13	1300	1300	Exchange stiffness, pJ/m
${L_{ex}}^*$	5.7	57	57	Exchange length, nm
${\delta_0}^{**}$	0.16	0.16	0.11	Bloch parameter, μm
L/L_{ex}	224	22.4	22.4	Exchange influence
q	0.23	0.23	0.5	Magnetic hardness

$$^*L_{ex} = \sqrt{\frac{2A}{\mu_0 {M_s}^2}} \quad ; \quad ^{**}\delta_0 = \sqrt{\frac{A}{K_u}}$$

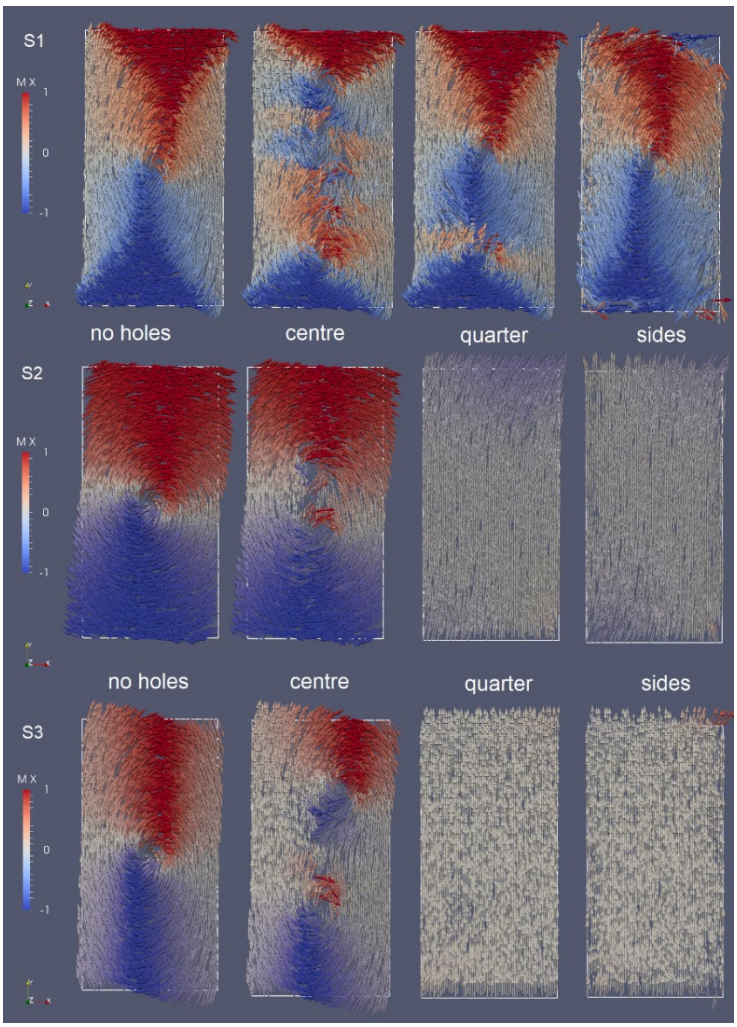

Figure 3. Relaxation results for various geometries from the initial state presented in Figure 2. Top panel for material S1 (weak exchange stiffness constant, week anisotropy); middle panel for material S2 (strong exchange constant but week anisotropy) and bottom panel for S3 (strong exchange stiffness constant and anisotropy). Magnetization vectors are coloured by M_x component.

In this part we present the comparison between three materials, to which we will be referring as S1, S2, and S3 (see Table 1), that have weak (S1) and strong (S2, S3) exchange stiffness constant. The intermediate material S2 has the same anisotropy constant as S1, and exchange stiffness constant of S3. The results of the relaxation process are presented in Figure 3. Here we can see that without any defects, the sample S1 shows the formation of 90° and 180° domain wall, whereas for the S2 and S3, the magnetization vectors take form of a single vortex.

If we now look at the results for geometry with defects, we can see that in the case where “holes” are normally distributed and concentrated in the center of the plate, creating non-magnetic clusters, the domain walls get distorted around these defects, due to the pinning of vortices. There is a quantitative difference between three materials, but qualitatively the picture is very similar.

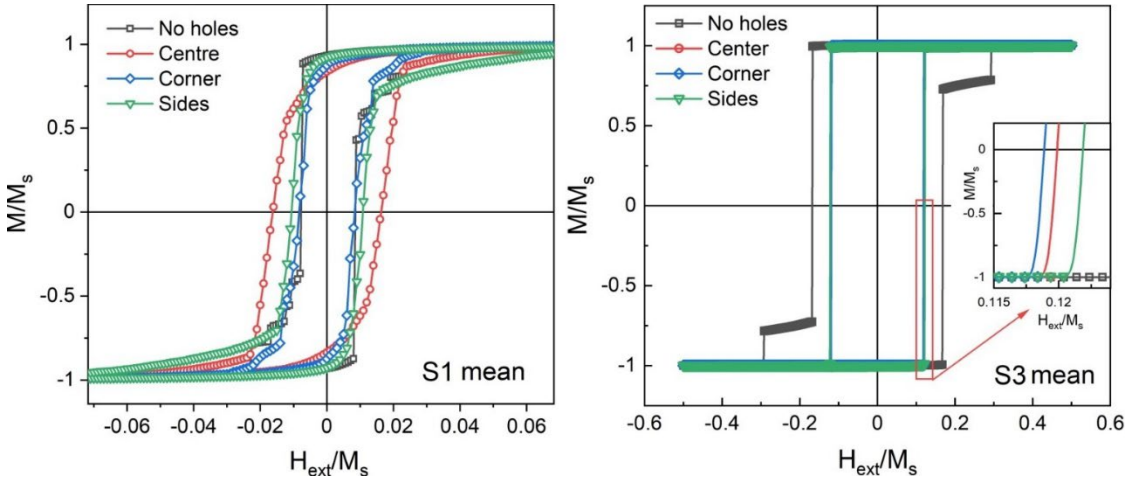

Figure 4. Average hysteresis cycle for materials S1 (left) and S3 (right), with weak and strong exchange stiffness constant, respectively. The corresponding configurations are given in legends. For better visibility the magnified zone of magnetization reversal for S3 are given in the insert.

However, the result changes drastically when the center of defects is shifted from energetically favorable position of vortices (center). For the soft material S1 we still observe the formation of the domain walls. Then, when we increase only the exchange parameter, for S2 we observe that the equilibrium state is a single domain. This means that, due to the strong exchange coupling, we reach a limit where the energy of domain walls is too high and the single-domain state is energetically more favorable. With additional increase of the anisotropy constant, the magnetization vectors align themselves perfectly with the easy axis direction (see Figure 3 for S3). The influence of the anisotropy constant is discussed in the next subsection.

The domain formation has a crucial impact on the magnetization process and coercive field. In order to determine the influence of the magnetic defects, we have simulated full hysteresis cycles for aforementioned configurations. To obtain the average picture, we run computations on 100 different patterns for each principal defects configurations. This means that the amount of defects stays the same, the probability of their position within the sample is the same (concentrated either in the center, quarter or sides) but the patterns are slightly different. Every hysteresis computation cycle starts from a saturated state and after two cycles comes to a stable and reproducible solution.

The resulting average hysteresis loops are plotted in Figure 4. The shape of the hysteresis cycle for S1 correspond to that of soft magnetic material [24, 25]. The small jumps in magnetization correspond to the unpinning of vortices. It is observed that the coercive field has the highest value when the defects are concentrated in the center, which means that the magnetic vortices get pinned on these defects, in agreement with the previous results [9, 26, 27].

Then, if we look at the results for material with strong exchange coupling, S3, we observe a completely different situation. The cycle has a squarer shape with the switching of magnetization for a given field. The value of switching field for pure material corresponds well to the results obtained by Stoner-Wohlfarth model. However, the presence of defects leads to premature nucleation and switching. This can be explained by the defects serving as nucleation points for the magnetization reversal [8]. The obtained results show that tailoring defect patters can be used to forecast the magnetic characteristics of single-domain ultra-thin magnetic films.

3.2 Variation of Domain Wall Width

In this subsection we compare the average hysteresis cycles with increasing anisotropy constant, i.e. decreasing domain wall width. In Figure 5 is displayed the comparison between coercive fields for given defect distribution and anisotropy constant (left axis) and respective domain wall width (right axis). The corresponding values are given in Table 2 and the highest value of coercive field H_c are in bold font as a guide for eyes. It is interesting, that in the situation where the domain wall's width is of the same size as the specimen width, the highest H_c corresponds to the cluster of defects located in the center.

However, when the domain walls become much smaller than the size of the plate, the coercive field becomes stronger in the situation, where the defects are located on the sides. This corresponds to the area with highest demagnetization field value and strong magnetization gradient. The configuration with defect cluster located in a corner displays the lowest H_c value throughout the studied range, as the small defects are located outside the area with strong magnetization gradient. They serve as nucleation points for the magnetization reversal process and have lower threshold for unpinning of the domain walls.

4. CONCLUSION

In this paper, using micromagnetic simulation, we investigated domain structure and magnetization processes of thin permalloy films with the in-plane uniaxial magnetic anisotropy. We have modelled numerically the magnetization process of two permalloy thin films with weak and strong exchange stiffness and crystalline anisotropy constants, and investigated the influence of non-magnetic defects on this process.

Table 2. Coercive fields and domain wall width for corresponding anisotropy constants

Anisotropy constant (J/m^3)	Bloch domain wall width (nm)	Coercive field (H_c/M_s)			
		Without defects	Defects in centre	Defects in corner	Defects in sides
500	596	0.00982	**0.0149**	0.00845	0.0109
1000	421	0.00982	**0.0162**	0.00861	0.0109
2000	298	0.0104	**0.0162**	0.00842	0.0114
4000	211	0.0114	**0.0164**	0.00854	0.0120
8000	149	0.0130	**0.0176**	0.00920	0.0140
16000	105	0.0172	**0.0204**	0.0120	0.0175
32000	75	0.0248	0.0258	0.0211	**0.0271**
64000	53	0.0425	0.0431	0.0409	**0.0490**

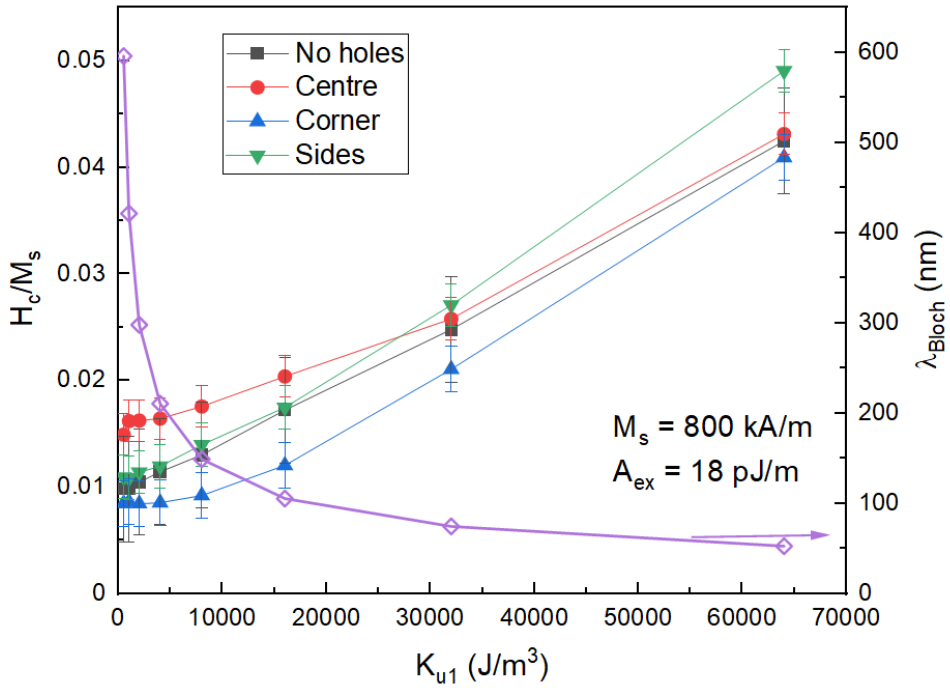

Figure 5. Dependence of coercive field (left) and Bloch (in-plane) domain wall width (right) on anisotropy constant. The corresponding defect configurations are given in legends. The magenta line with diamonds represents the Bloch domain wall width variation.

It is shown that the geometry of non-magnetic defects distribution plays different roles depending on the domain wall and exchange length scales. In the case of a soft magnetic material with lower exchange length and large domain walls it was shown that defects pin magnetic vortices and increase coercive field. The maximum coercive field is observed when the defects are located in the center. On the other side, in the case of hard magnetic material with high exchange stiffness constant, it was shown that defects, that are shifted from the center, favor a single-domain state. The magnetization reversal happens instantly at a given switching field. The value of this field is higher when there are no defects and the hysteresis curve has an intermediate step, that corresponds to the creation and moving of a domain wall. The defects create singularity points for magnetization vortices and serve as nucleation centers for the magnetization reversal therefore the switching field has lower values.

We studied the influence of a domain wall width on the magnetization process of a soft magnetic material. It was shown that the increase in anisotropy leads to a remarkable rise of the coercive field. It was shown, that when the domain wall width becomes smaller than the size of the sample, the higher H_c is observed in the case of defects located at the sides of the sample. It is shown that small defects, located outside of the singularity points for magnetization vortices, display the lowest unpinning energy and serve as nucleation points for magnetization reversal.

The presented study might be of particular interest for modelling and predictions of magnetic properties of permalloy and, potentially, for developers of practical devices based on ferromagnetic thin films.

ACKNOWLEDGMENT

The work described in the present paper has been developed within the project “Online Microstructure Analytics” (Ref. OMA,

Grant Agreement No. 847296) that has received funding from the Research Fund for Coal and Steel of the European Union, which is gratefully acknowledged. The sole responsibility of the issues treated in the present paper lies with the authors; the Commission is not responsible for any use that may be made of the information contained therein.

REFERENCES

[1] S. Parkin, X. Jiang, C. Kaiser, A. Panchula, K. Roche and M. Saman, Magnetically engineered spintronic sensors and memory, *Proceedings of the IEEE*, 91, 2003, 661-680.
[2] D. A. Allwood, G. Xiong, C. C. Faulkner, D. Atkinson, D. Petit and R. P. Cowburn, Magnetic domain-wall logic, *Science*, 309, 2005, 688-1692.
[3] C. Chappert, A. Fert and F. V. Dau, The emergence of spin electronics in data storage, *Nature Materials*, 6, 2007, 813-823.
[4] T. L. Jin, M. Ranjbar, S. K. He, W. C. Law, T. J. Zhou, W. S. Lew, X. X. Liu and S. N. Piramanayagam, Tuning magnetic properties for domain wall pinning via localized metal diffusion, *Scientific Reports*, 7, 2017, 1-7.
[5] S. Parkin and S. H. Yang, Memory on the racetrack, *Nature Nanotech*, 10, 2015, 195-198.
[6] R. D. Shull, Y. P. Kabanov, V. S. Gornakov, P. J. Chen and V. I. Nikitenko, Shape critical properties of patterned Permalloy thin films, *Journal of Magnetism and Magnetic Materials*, 400, 2016, 191-199
[7] M. C. Giordano, S. E. Steinvall, S. Watanabe, A. F. Morral and D. Grundler, $Ni_{80}Fe_{20}$ nanotubes with optimized spintronic functionalities prepared by atomic layer deposition, *Nanoscale*, 13, 2021, 13451-13462.
[8] A. Hubert and R. Schaefer, *Magnetic domains: The analysis of magnetic microstructures*. Berlin, Heidelberg: Springer Verlag, 2009.
[9] D. Toscano, J. Silva, P. Z. Coura, R. A. Dias, B. V. Costa and S. A. Leonel, Magnetic vortex behavior and its dynamics in nano-magnets in the presence of impurities, *Physics Procedia*, 28, 2012, 99-104.
[10] T. Takashita, N. Nakamura and Y. Ozaki, Influence of iron powder properties on hysteresis loss of iron powder core, *JFE technical report*, 21, 2016, 78-84.
[11] W. Brown Jr., *Micromagnetics*, John Wiley and Sons, 1963.
[12] W. Döring, *Micromagnetics, Physics Handbook*, Springer, USA, 1966.
[13] J. Fidler and T. Schrefl, Micromagnetic modelling - the current state of the art, *Journal of Physics D: Applied Physics*, 33, 2000, 135-156.
[14] I. Betancourt, G. Hrkac and T. Schrell, Micromagnetic simulation of domain wall dynamics in permalloy nanotubes at high frequencies, *Journal of Applied Physics*, 104, 2008, 023915.
[15] B. Belyaev and A. Izotov, Micromagnetic calculation of magnetostatic oscillation modes of an orthogonally magnetized disk of yttrium iron garnet, *Physics of the Solid State*, 55, 2013, 2491-2500.
[16] J. Leliaert and J. Mulkers, Tomorrow's micromagnetic simulations, *Journal of Applied Physics*, 125, 2019, 180901.
[17] B. Belyaev, A.V. Izotov, G. V. Skomorokhov and P. N. Solovev, Micromagnetic analysis of edge effects in a thin magnetic film during local excitation of magnetization oscillations, *Russian Physics Journal*, 63, 2020, 837-843.
[18] L. Landau and E. Lifshitz, On the theory of the dispersion of magnetic permeability in ferromagnetic bodies, *Phys Z Sowjetunion*, 8, 1935, 153-169.
[19] S. Labbé, *Numerical simulation of high-frequency behavior of ferromagnetic materials*, Ph.D. Dissertation, University Paris 13, Paris, France,1998.
[20] S. Labbé and P. Leca, Fast solver for the Maxwell quasistatic equations: block-Toeplitz matrix, Application to micromagnetism, *CR Acad Sci Paris*, 327, 1998, 415-420.
[21] S. Labbé and P. Y. Bertin, Microwave polarizability of ferrite particles with non-uniform magnetization, *Journal of Magnetism and Magnetic Materials*, 206, 1999, 93-105.
[22] S. Labbé, Fast computation for large magnetostatic systems adapted for Micromagnetism, *SIAM Journal of Scientific Computing*, 26, 2005, 2160-2175.
[23] D. Lee, Fast multiplication of a recursive block Toeplitz matrix by a vector and its application, *Journal of Complexity*, 2, 1986, 295-305.
[24] E. Pellicer, E. Rossinyol, M. Cabo, A. Lopez-Ortega and M. Estrader, Oxide-matrix based nanocomposite materials for advanced magnetic and optical functionalities, in *Advances in Nanocomposites - Synthesis, Characterization and Industrial Applications*, InTech, 2011, 343-358.
[25] X. Wen, S. Kelly, J. Andrew and D. Arnold, Nickel-zinc ferrite/permalloy ($Ni_{0.5}Zn_{0.5}Fe_2O_4$/Ni Fe) soft magnetic-nanocomposites fabricated by electro-infiltration, *AIP Advances*, 6, 2016, 056111.
[26] M. Rahm, J. Biberger, V. Umansky and D. Weiss, Vortex pinning at individual defects in magnetic nanodisks, *Journal of Applied Physics*, 93, 2003, 7429-7431.
[27] M. Rahm, J. Stahl, W. Wegscheider and D. Weiss, Multistable switching due to magnetic vortices pinned at artificial pinning sites, *Applied Physics Letters*, 85, 2004, 1553-1555.